POLITECNICO DI TORINO
Repository ISTITUZIONALE

Finite element models with node-dependent kinematics based on Legendre polynomials for the global–local analysis of compact and thin walled beams

Original
Finite element models with node-dependent kinematics based on Legendre polynomials for the global–local analysis of compact and thin walled beams / Zappino, E., Scano, D., Carrera, E.. - In: COMPUTER METHODS IN APPLIED MECHANICS AND ENGINEERING. - ISSN 0045-7825. - 415:(2023). [10.1016/j.cma.2023.116212]

Availability:
This version is available at: 11583/2996631 since: 2025-01-16T10:33:48Z

Publisher:
Elsevier

Published
DOI:10.1016/j.cma.2023.116212

Terms of use:

This article is made available under terms and conditions as specified in the corresponding bibliographic description in the repository

Publisher copyright
Elsevier postprint/Author's Accepted Manuscript

© 2023. This manuscript version is made available under the CC-BY-NC-ND 4.0 license
http://creativecommons.org/licenses/by-nc-nd/4.0/.The final authenticated version is available online at:
http://dx.doi.org/10.1016/j.cma.2023.116212

(Article begins on next page)

17 June 2026

Finite element models with node-dependent kinematics based on Legendre polynomials for the global-local analysis of compact and thin walled beams

E. Zappino[*], D. Scano [†], E. Carrera [‡]

Mul^2 Group
Department of Mechanical and Aerospace Engineering, Politecnico di Torino
Corso Duca degli Abruzzi 24, 10129 Torino, Italy.

Abstract: *In the present work, enhanced one-dimensional finite elements with node-dependent kinematics are proposed for the static analysis. Finite element governing equations are derived by applying the Carrera Unified Formulation. This framework subdivides the three-dimensional displacement field into a cross-section domain and an axis domain. The dimension along the beam is discretized by using Lagrange-based shape functions. At each node of the element, an independent structural theory can be imposed, thus obtaining a node-dependent kinematic model. This method permits to focus on the finite element node. In this way, several combinations of kinematics can be used together. In particular, Taylor-based and Legendre-based expansions have been adopted in this paper to create global-local models without using special coupling methods. The results have been compared with well-established benchmarks from the literature. Compact section and thin-walled beams have been taken into account. Results have been given in terms of displacements and stresses. It is shown that the present model provides high accuracy with a reduced number of degrees of freedom.*

Keywords: Carrera Unified Formulation; beam models; Node-dependent kinematics; Legendre polynomials; Taylor polynomials.

1 Introduction

The development of next-generation structures requires the implementation of advanced computational tools which can accurately study cumbersome problems and provide increasingly accurate results. However, these tasks lead to an exponential rise in computational costs. In order to keep them in reasonable ranges, several approaches have been developed in the last decades. For instance, one of the most used methods adopts refined models in regions where higher-order effects must be analyzed, see Reddy [1]. Contrarily, the rest of the structure is discretized by low fidelity models.

[*]Assistant Professor. E-mail: enrico.zappino@polito.it
[†]PhD Student. E-mail: daniele.scano@polito.it
[‡]Professor of Aeronautics and Astronautics. E-mail: erasmo.carrera@polito.it

Many beam models have been proposed. First, the classical Euler-Bernoulli [2] beam model deserves to be mentioned, which does not account for the shear effects. It is able to study isotropic slender structures. The other classical theory is the Timoshenko [3] beam model, which can capture the shear effects. However, more refined models are needed if sophisticated behaviours have to be captured, as described in the influential book by Novozhilov [4]. Comprehensive reviews of advanced beam models are given in Kapania and Raciti [5, 6] and Carrera *et al.* [7]. Advanced one-dimensional (1D) models aim to overcome the limitations of classical beam theories. For instance, the use of warping functions was proposed by Vlasov [8] to take the cross-section deformation into account. Thanks to this method, thin-walled structures were analysed by Friberg [9], Ambrosini *et al.* [10] and Mechab *et al.* [11]. Generalized Beam Theory (GBT) was proposed by Schardt [12]. This method expands the displacement field of the cross-section thin-walled beam. Berdichevsky [13] proposed the Variation Asymptotic Method (VAM). An asymptotic expansion of the solution is built by using a characteristic cross-section parameter. Giavotto *et al.* [14] further adopted this method. Živković *et al.* [15] introduced a general beam formulation which includes the cross-sectional deformation. Yoon and Lee [16] proposed a similar approach that is able to study in- and out-of-plane warping. Reda *et al.* [17] elaborated an enhanced Timoshenko microstructured beam when tetrachiral structures are employed. Alavi *et al.* [18] proposed a linear size-dependent Timoshenko beam model that is based on the consistent couple stress theory. Bousselmi *et al.* [19] illustrated new enriched beam models to account for the cross-section higher-order phenomena. Finally, Carrera Unified Formulation (CUF) must be mentioned, which was initially proposed by Carrera [20]. Carrera and Giunta [21] extended the use of CUF for the beam formulation. In this framework, it is possible to approximate the cross-section kinematics with every kind of function.

The previous beam models improve the accuracy of the solutions, but the computational costs significantly increase. For instance, local effects such as delamination [22], cracks [23], or local buckling [24] require a refined local solution. Thus, it would be beneficial to use very refined models in specific regions with non-classical effects while the other parts of the structures could be modelled with low fidelity models. In this way, the computational costs can be reduced, while maintaining a good accuracy of the solution. In the last decades, several efforts have been made to implement global-local analysis methods. Noor [25] reviewed

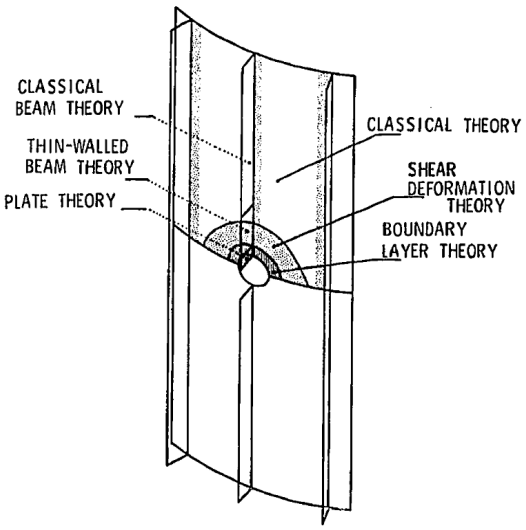

Figure 1: Global-local approach for a blade stiffened panel, reported from [25].

several global-local methodologies. In particular, regarding the possibility to adopt refined and lower models, Noor stated: *[...]The effective implementation of this approach requires the following:*

1. *systematic procedure for generating the hierarchy of mathematical models[...],*
2. *criteria for the adaptive refinement of the mathematical model, and*
3. *treatment of the interfaces between the different regions.*

Figure 1 shows a blade stiffened panel with a cut-out, analyzed with different theories a the same time.
Many issues arise when the compatibility of the displacements between two different computational domains must be enforced. For instance, Fish *et al.* [26] developed a multi-grid method for sharing information between coarse and fine meshes by adopting an iterative algorithm. One of the most adopted methods is the use of Lagrange multipliers, see Prager [27]. In this context, Park and Felippa [28] proposed a continuum-based variational principle for formulating discrete governing equations of partitioned structural systems. Carrera *et al.* [29] used this approach in the beam formulation for CUF. In this work, Taylor expansions with different polynomial orders are combined. Furthermore, Aminpour et al. [30], and Ransom [31] employed a spline method to couple two domains with different meshes. Brezzi and Marini [32] proposed a similar approach in the framework of the three-field formulation. An eXtended Variational Formulation (XVF) was proposed by Blanco *et al.* [33, 34]. This method couples different kinematic models by using the Lagrange multiplier approach.
The compatibility between two zones can be imposed by using an overlapping zone. In particular, Ben Dhia [35] and Ben Dhia and Rateau [36] suggested the Arlequin method with Lagrange multipliers. This approach was adopted in the framework of CUF by Biscani *et al.* for beam models [37] and plate models [38]. The Arlequin method was used by Hu *et al.* [39, 40] in the linear and non-linear multi-scale analysis of sandwich structures.
Furthermore, Klarmann *et al.* [41] coupled beam and solid elements. The solid part considers cross-sectional deformation, while the beam elements account for the rigid body movement of the cross-section exclusively. Hartloper *et al.* [42] proposed a warping-inclusive kinematic coupling method in the framework of FEM to study thin walled structures. Zappino and Carrera *et al.* [43] treated complex geometries with the coupling of 3D, 2D and 1D models in the framework of the CUF for the dynamic and static analyses of a complete aircraft, respectively.
Following Noor's prescriptions, the present work intends to illustrate the capabilities of the Node-Dependent Kinematics (NDK) approach implemented for one-dimensional formulation in the CUF framework. Legendre-Legendre and Legendre-Taylor combinations are used. The axis is discretized by one-dimensional finite elements, whereas the cross-section is described by different expansions for each element node. In particular, Lagrange-based shape functions are used along the beam axis, whereas Taylor or Legendre-based expansions are adopted as higher-order kinematics assumptions over the cross-section. Thanks to the scalable nature of CUF, the desired theory of structures can be chosen for each element node without using other mathematical equations. In particular, for a 1D problem, the expansion functions are changed along the beam axis. Using the Finite Element Method (FEM), there are no issues in joining different structural theories. The 1D governing equations of the beam theory are obtained via the so-called fundamental nuclei. In this way, low- to higher-order theory can be arbitrarily employed. This approach was first proposed by Carrera and Zappino [44] for linear static analysis. Lagrange-like and Taylor-like expansions are adopted over the cross-section.

Li *et al.* [45] used Legendre and Taylor expansions adopted in the same FE models. Moleiro *et al.* [46] introduced the NDK method in the Reissner Mixed Variational Method (RMVT). This paper is structured as follows: Section 2 reviews the Hierarchical Legendre Expansions for the beam formulation. Section 3 illustrates the beam formulation for CUF. Furthermore, this Section presents the Node-Depenedent Kinematics method and the governing equations. Finally, the assembly of the stiffness matrix is illustrated. Section 4 presents the results for end-effects on compact section and thin-walled beam. Finally, Section 5 draws the most relevant conclusions of this work.

2 One-dimensional models based on Hierarchical Legendre polynomials

2.1 Recurrence relations

In the present work, the Legendre polynomials are used to build Hierarchical Legendre Expansion (HLE) as structural theories. The theoretical background is presented by Szabo and Babuška [47]. The main feature is that they combine the hierarchy in the structure of the kinematic terms (as for TE) with a non-local distribution of the mechanical unknowns over the cross-section domain (as for LE). Moreover, they are built from the same cross-section discretisation, and other functions are adopted (hp-method for CUF). In order to obtain the HLE expansions in the cross-section of a beam, one-dimensional Legendre polynomials can be expressed in the following relation:

$$L_p(\zeta) = \frac{2p+1}{p+1} L_{p-1}(\zeta) - \frac{p}{p+1} L_{p-2}(\zeta), \qquad p = 2, 3, ... \tag{1}$$

where p indicates the polynomial order. The relation is valid in the natural plane $\zeta = [-1, +1]$. The initial values are $L_0(\zeta) = 1$ and $L_1(\zeta) = \zeta$. A set of 1D functions can be defined out of these polynomials as:

$$\begin{aligned} \tilde{L}_1(r) =& \frac{1}{2}(1-r) \\ \tilde{L}_2(r) =& \frac{1}{2}(1+r) \\ \tilde{L}_i(r) =& \phi_{i-1}(r), \quad i = 3, 4, ..., p+1 \end{aligned} \tag{2}$$

with

$$\phi_j(r) = \sqrt{\frac{2j-1}{j}} \int_{-1}^{r} L_{j-1}(\zeta) d\zeta = \sqrt{\frac{1}{4j-1}} \left(L_j - L_{j-2} \right), \quad j = 2, 3, ..., p \tag{3}$$

This Legendre-based set of functions maintains the orthogonal properties of the Legendre polynomials:

$$\int_{-1}^{1} \frac{\tilde{L}_i}{\mathrm{d}r} \frac{\tilde{L}_i}{\mathrm{d}r} \mathrm{d}x = \delta_{ij}, \quad \text{for } i \geq 3 \text{ and } j \geq 1 \tag{4}$$

Finally, Legendre polynomials are a particular type of Jacobi polynomials. See Abramowitz and Stegun [48] for more information.

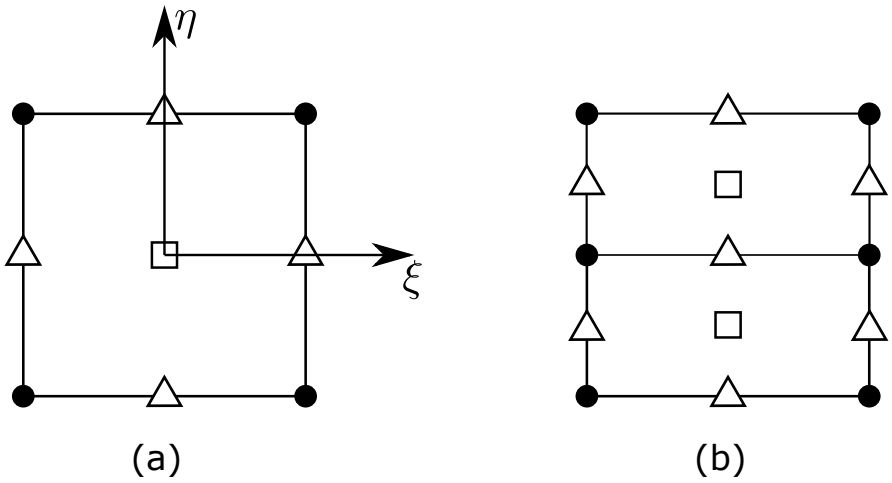

Figure 2: Hierarchical Legendre Expansions for beam. Definition of vertexes ● edges △ and faces □. Natural plane (a) and multi-domain cross-section discretization (b).

2.2 Hierarchical Legendre Expansion

Four this expansion, three kinds of interpolation functions are adopted over the domain, namely vertex, edge and internal polynomials.
Fig. 2 (a) shows an illustration of the beam cross-section in the natural plane with $\xi = [-1, +1]$ and $\eta = [-1, +1]$. Fig. 2 (b) illustrates a multi-domain discretization of the cross-section. The vertex modes are four, one per vertex, and they vanish at all nodes but one. Secondly, the edge modes vanish for all sides of the domain but one. Finally, the internal modes vanish at all sides, and they are just included from the fourth order expansion and higher.

Vertex expansions The vertex modes correspond to the first-order, quadrilateral Lagrange polynomials:

$$F_\tau(\xi, \eta) = \frac{1}{4}(1 - \xi_\tau \xi)(1 - \eta_\tau \eta), \quad \tau = 1, 2, 3, 4 \tag{5}$$

where ξ and η vary above the domain between -1 and +1, and ξ_τ and η_τ represent the vertex coordinates in the natural plane. In Fig. 3 (a), F_1 vertex expansion is shown.

Edge expansions The edge modes are defined for $p \geq 2$ in the natural plane as follows

$$\begin{aligned}
F_\tau(\xi, \eta) =& \frac{1}{2}(1 - \eta)\,\phi_p(\xi), \quad \tau = 5, 9, 13, 18, ... \\
F_\tau(\xi, \eta) =& \frac{1}{2}(1 + \xi)\,\phi_p(\eta), \quad \tau = 6, 10, 14, 19, ... \\
F_\tau(\xi, \eta) =& \frac{1}{2}(1 + \eta)\,\phi_p(\xi), \quad \tau = 7, 11, 15, 20, ... \\
F_\tau(\xi, \eta) =& \frac{1}{2}(1 - \xi)\,\phi_p(\eta), \quad \tau = 8, 12, 16, 21, ...
\end{aligned} \tag{6}$$

where p represents the polynomial degree of the bubble function. It is possible to note that the above functions are expressed in such a way that they satisfy the side-continuity in multi-domain beam theories. In Fig. 3 (b), F_9 edge expansion is illustrated.

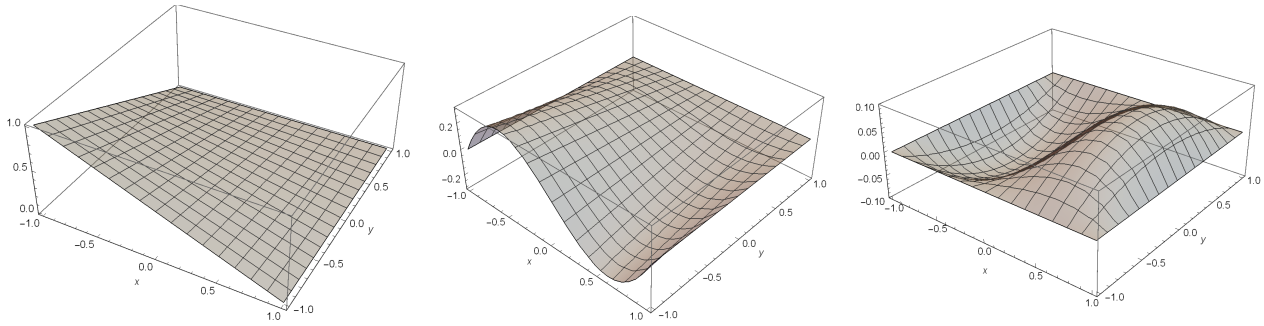

(a) (b) (c)

Figure 3: Vertex expansions (a), edge expansion (b) and internal expansion (c).

Internal expansions F_τ internal expansions (also known as bubble functions) are built by multiplying 1D edge modes. They are purely local. They are able to account for higher-order and localized phenomena. There are $(p-2)(p-3)/2$ internal polynomials for $p \geq 4$, and they vanish at all the edges of the quadrilateral. The general τ-th expansion is built by using the following expansion:

$$F_\tau = \phi_i(\xi)\phi_j(\eta) \quad i,j \geq 2 \text{ with } i+j=p \tag{7}$$

For instance, considering the set of fifth-order polynomials, it contains 3 internal expansions, which are

$$\begin{aligned} F_{17}(\xi,\eta) =& \phi_2(\xi)\phi_2(\eta), \quad 2+2=4 \\ F_{22}(\xi,\eta) =& \phi_3(\xi)\phi_2(\eta), \quad 3+2=5 \\ F_{23}(\xi,\eta) =& \phi_2(\xi)\phi_3(\eta), \quad 2+3=5 \end{aligned} \tag{8}$$

In Fig. 3 (c), F_{22} internal expansion is displayed.

3 Node-dependent kinematics one-dimensional models

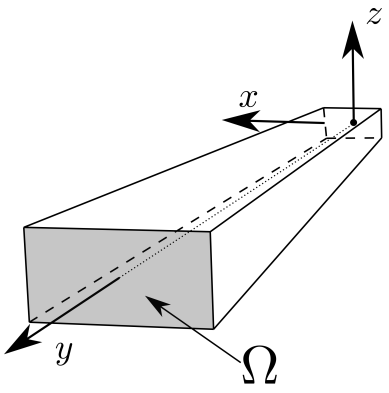

Figure 4: Reference system for a beam.

3.1 Preliminaries

Let us consider a beam in Fig. 4. The beam axis is aligned along the y direction, while the cross-section domain Ω lies in the (x,z)-plane. The three-dimensional displacement vector

for a multi-domain section beam in this reference system can be expressed as:

$$\mathbf{u}^k(x,y,z) = \left\{ \begin{array}{ccc} u_x^k(x,y,z) & u_y^k(x,y,z) & u_z^k(x,y,z) \end{array} \right\}^T \tag{9}$$

The strain, $\boldsymbol{\epsilon}^k$, and stress, $\boldsymbol{\sigma}^k$, components are herein arranged as:

$$\boldsymbol{\sigma}^k = \left\{ \begin{array}{cccccc} \sigma_{xx}^k & \sigma_{yy}^k & \sigma_{zz}^k & \sigma_{xz}^k & \sigma_{yz}^k & \sigma_{xy}^k \end{array} \right\}^T, \quad \boldsymbol{\epsilon}^k = \left\{ \begin{array}{cccccc} \epsilon_{xx}^k & \epsilon_{yy}^k & \epsilon_{zz}^k & \epsilon_{xz}^k & \epsilon_{yz}^k & \epsilon_{xy}^k \end{array} \right\}^T \tag{10}$$

where the strain vector are related to the displacements through the differential operator matrix $\mathbf{D}$ as

$$\boldsymbol{\epsilon}^k = \mathbf{D}\mathbf{u}^k \tag{11}$$

For problems with infinitesimal strains, $\mathbf{D}$, in an explicit form is:

$$\mathbf{D} = \begin{bmatrix} \partial_x & 0 & 0 \\ 0 & \partial_y & 0 \\ 0 & 0 & \partial_z \\ \partial_z & 0 & \partial_x \\ 0 & \partial_z & \partial_y \\ \partial_y & \partial_x & 0 \end{bmatrix} \tag{12}$$

where $\partial_x = \dfrac{\partial(\cdot)}{\partial x}$, $\partial_y = \dfrac{\partial(\cdot)}{\partial y}$ and $\partial_z = \dfrac{\partial(\cdot)}{\partial z}$.
The stress components can be attained by means of the constitutive equation as follows:

$$\boldsymbol{\sigma}^k = \tilde{\mathbf{C}}^k \boldsymbol{\epsilon}^k \tag{13}$$

where $\tilde{\mathbf{C}}^k$, is the matrix of the material coefficients.
In the framework of CUF, the 3D displacement field and the related virtual variation can be conveniently written as follows

$$\begin{array}{rcll} \mathbf{u}^k(x,y,z) & = & F_\tau(x,z)\mathbf{u}_\tau^k(y), & \tau = 1,\ldots,M \\ \delta\mathbf{u}^k(x,y,z) & = & F_s(x,z)\delta\mathbf{u}_s^k(y), & s = 1,\ldots,M \end{array} \tag{14}$$

where $F_\tau(x,z)$ are the expansion functions over the cross-section, the Einstein convention with the repeated index τ is assumed, and M is the total number of expansions used. Thanks to this formulation, it is possible to adopt an infinite number of structural theories. For the sake of simplicity, Legendre-like and Taylor-like functions are presented. In this paper, Taylor-like expansions are used in the *global* zone. For the beam formulation, Taylor expansion uses 2D polynomials $x^i z^j$ as the base, where i and j are positive integers. Carrera and Giunta [21] firstly studied beams from the first (T1) to the fourth (T4) orders to account for non-classical effects.
Then, the axial displacement vector, $\mathbf{u}_\tau^k$, and the virtual variation, $\delta\mathbf{u}_s^k$, can be approximated with the Finite Element Method (FEM) as follows:

$$\begin{array}{rcll} \mathbf{u}_\tau^k(x,y,z) & = & N_i(y)\mathbf{u}_{\tau i}^k(y), & i = 1,\ldots,N_n \\ \delta\mathbf{u}_s^k(x,y,z) & = & N_j(y)\delta\mathbf{u}_{sj}^k(y), & j = 1,\ldots,N_n \end{array} \tag{15}$$

in which $N_i(y)$ are the shape functions, and N_n the number of nodes within an element, $\mathbf{u}^k_\tau(x,y,z)$ the nodal unknowns. In this work, the classical four-node Lagrange (B4) element is considered for the numerical assessments. See Bathe [49] for more information.
Thus, by using the CUF approximation (Eq. (14)) and the FEM discretization (Eq. (15)), it is possible to write the complete expression of FE displacement functions:

$$\begin{array}{rcll} \mathbf{u}^k(x,y,z) & = & N_i(y)F_\tau(x,z)\mathbf{u}^k_{\tau i}(y), & \tau = 1,\ldots,M; \quad i = 1,\ldots,N_n \\ \delta\mathbf{u}^k(x,y,z) & = & N_j(y)F_s(x,z)\delta\mathbf{u}^k_{sj}(y), & s = 1,\ldots,M; \quad j = 1,\ldots,N_n \end{array} \tag{16}$$

3.2 Node-Dependent Kinematics

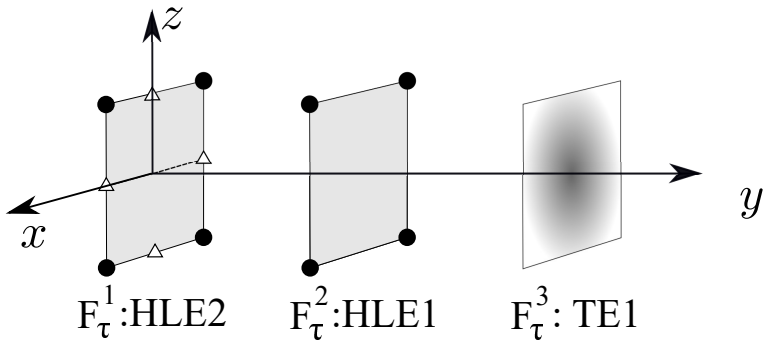

Figure 5: A three-node beam element with node-dependent kinematics.

A further step can be made if the cross-sections functions are *anchored* to the nodes of beam elements. Substantially, each FE node has its own structural theories. This concept can be summarized mathematically in the followings:

$$\begin{array}{rcll} \mathbf{u}^k(x,y,z) & = & N_i(y)F^i_\tau(x,z)\mathbf{u}^k_{\tau i}(y), & \tau = 1,\ldots,M_i; \quad i = 1,\ldots,N_n \\ \delta\mathbf{u}^k(x,y,z) & = & N_j(y)F^j_s(x,z)\delta\mathbf{u}^k_{sj}(y), & s = 1,\ldots,M_j; \quad j = 1,\ldots,N_n \end{array} \tag{17}$$

Eq. (17) describes a family of one-dimensional FE models with NDK. Thus, in this kind of element, different kinematics can be adopted in the same element straightforwardly. In this approach, a local kinematic refinement on the nodal level can be conveniently carried out. In particular, Fig. 5 shows a B3 element, where three different theories are adopted. Taylor-like and Legendre-like expansions can be easily used without mathematical artifices. In the first node, HLE2 has eight expansions, and the kinematic model for u_x is written as

$$u_x(x,y,z) = F^1_1 u_{x_1} + F^1_2 u_{x_2} + F^1_3 u_{x_3} + F^1_4 u_{x_4} + F^1_5 u_{x_5} + F^1_6 u_{x_6} + F^1_7 u_{x_7} + F^1_8 u_{x_8} \tag{18}$$

The total number of Degrees Of Freedom (DOF) for the first node is given by 8×3, since there are eight expansions and three displacement fields. u_y and u_z can be written with an analogous procedure. On the other hand, HLE1 is associated to four expansions. The u_x displacement field has the following shape:

$$u_x(x,y,z) = F^2_1 u_{x_1} + F^2_2 u_{x_{22}} + F^2_3 u_{x_3} + F^2_4 u_{x_4} \tag{19}$$

In this case, the number of DOF is $4{\times}3$. Finally, TE1 has three expansions and u_x can be written as follows:

$$u_x(x,y,z) = F^3_1 u_{x_1} + F^3_2 u_{x_2} + F^3_3 u_{x_3} \tag{20}$$

For the third node, the number of DOF is 3×3. At the end of the process, it is possible to write the u_x displacement field for the element

$$u_x(x,y,z) = N_1 F_\tau^1 u_{x_{\tau 1}} + N_2 F_\tau^2 u_{x_{\tau 2}} + N_2 F_\tau^2 u_{x_{\tau 2}} \tag{21}$$

or the complete field

$$\begin{aligned} u_x(x,y,z) = N_1(F_1^1 u_{x_{11}} + F_2^1 u_{x_{21}} + F_3^1 u_{x_{31}} + F_4^1 u_{x_{41}} + F_5^1 u_{x_{51}} + F_6^1 u_{x_{61}} + F_7^1 u_{x_{71}} \\ + F_8^1 u_{x_{81}}) + N_2(F_1^2 u_{x_{12}} + F_2^2 u_{x_{22}} + F_3^2 u_{x_{32}} + F_4^2 u_{x_{42}}) + N_3(F_1^3 u_{x_{13}} + F_2^3 u_{x_{23}} + F_3^3 u_{x_{33}}) \end{aligned} \tag{22}$$

The total number of DOF is the sum of the DOF of each node. In this way, there are $(8 \times 3 + 4 \times 3 + 3 \times 3) = 45$ degrees of freedom.

3.3 FE governing equations

The principle of virtual displacements is used to derive the governing equations:

$$\delta L_{int} = \delta L_{ext} \tag{23}$$

where δL_{int} represents the virtual variation of the internal work, while δL_{ext} indicates the virtual variation of the external work. δL_{int} can be expressed as:

$$\delta L_{int} = \int_{V_k} \delta \boldsymbol{\epsilon}^T \boldsymbol{\sigma} dV_k \tag{24}$$

By using the CUF-type displacement functions (Eq. 17), the geometric relations in Eq. 11, and constitutive equations (Eq. 13), the following expression can be obtained:

$$\delta L_{int} = \delta \mathbf{u}_{sj}^{kT} \int_{V_k} N_j F_s^j \mathbf{D}^T \tilde{\mathbf{C}}^k \mathbf{D} F_\tau^i N_i dV_k \mathbf{u}_{\tau i}^k = \delta \mathbf{u}_{sj}^{kT} \mathbf{K}_{ij\tau s}^k \mathbf{u}_{\tau i}^k \tag{25}$$

where $\mathbf{K}_{ij\tau s}^k$ is the Fundamental Nucleus (FN) of stiffness matrix for NDK FE models. The explicit expression of $\mathbf{K}_{ij\tau s}^k$ reads:

$$\mathbf{K}_{ij\tau s}^k = \int_{V_k} N_j F_s^j \mathbf{D}^T \tilde{\mathbf{C}}^k \mathbf{D} F_\tau^i N_i dV_k \tag{26}$$

The virtual work δL_{ext} done by the external load $\mathbf{p}$ is:

$$\delta L_{ext} = \int_{V_k} \delta \mathbf{u}^{kT} \mathbf{p}^k dV_k \tag{27}$$

The above equation can be further written in the form of CUF as:

$$\delta L_{ext} = \delta \mathbf{u}_{sj}^{kT} \int_{V_k} N_j F_s^j \mathbf{p}^k dV_k = \delta \mathbf{u}_{sj}^{kT} \mathbf{P}_{sj}^k \tag{28}$$

where $\mathbf{P}_{sj}^k$ represents the FN of the load vector. Hence, the governing equation for 1D FE models with NDK is described by the following relation:

$$\mathbf{K}_{ij\tau s}^k \mathbf{u}_{\tau i}^k = \mathbf{P}_{sj}^k \tag{29}$$

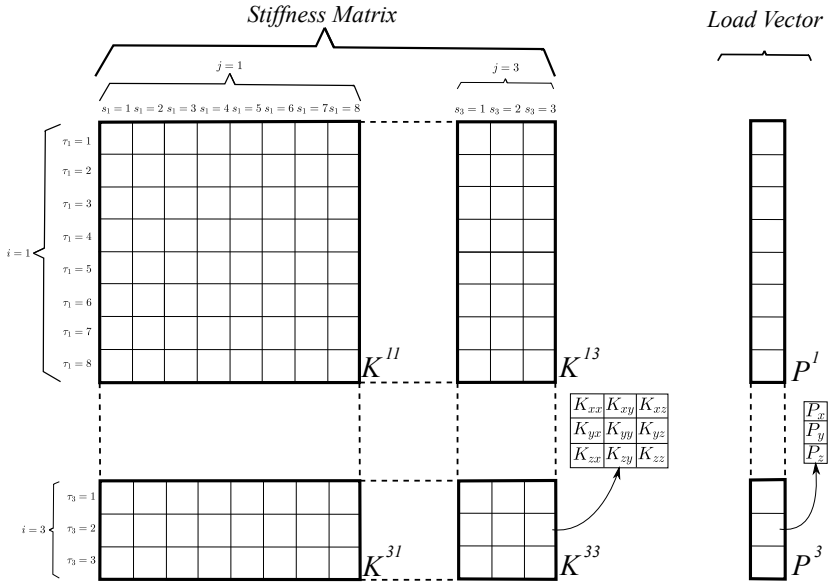

Figure 6: Assembly of the stiffness matrix and load vector of models with node-dependent kinematics.

3.4 Assembly of the stiffness matrix

In the previous section, the fundamental nucleus is indicated to be the 3×3 core unit of the stiffness matrix. On the other hand, FN of the load vector is 3×1. By looping on the indexes, the stiffness matrix on the node and element level can be obtained, then further assembled on the structure level. Carrera *et al.* [50] illustrated this process in an extended way.
Fig. 6 shows a part of the assembly of the stiffness matrix and load vector of models with node-dependent kinematics for the example already illustrated in Fig. 5. When different models are used within one element, K^{ij} is rectangular rather than square if $M_i \neq M_j$. For example, the number of expansion terms on node 1 is $M_1 = 8$, while for the third node $M_3 = 3$. The dimension of K^{11} is 24×24, K^{33} is a 9×9 matrix and K^{13} is a 24×9 while K^{31} a 9×24. The load vector must be built accordingly to the stiffness matrix.

4 Numerical results

In this section, displacement and stress fields are studied for two benchmarks. They are compared with reference solutions from the open literature. The first is a beam with a rectangular section, while the second is represented by an isotropic thin-walled C-section beam. The first example considers the end-effects near the clamped section for bending and traction loads. The second benchmark investigates transverse displacements and stresses near the loading point.
Different variable kinematic models have been considered and compared. The models have been named as follows:

1. HLEm indicates Hierarchical Legendre Expansion. This model permits to discretize the cross-section through several domains. This is useful in thin-walled structures to describe local phenomena;

2. TEm stands for Taylor Expansion, and m is the polynomial order. In this models family, it is not possible to accurately describe the geometry of the section. The only way to

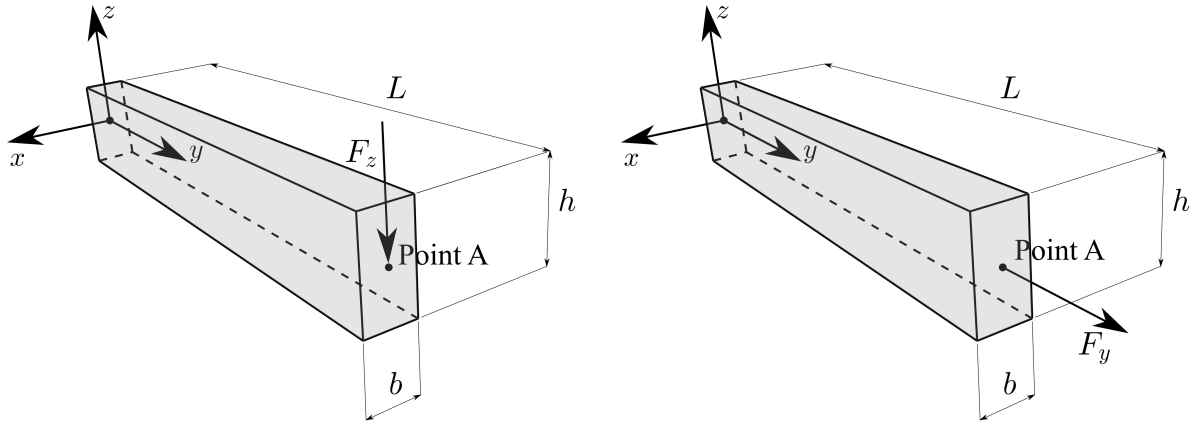

(a) Transverse Load (b) Traction Load

Figure 7: Geometrical properties of the cantilever beam with compact section. The study case is taken from [51] and [52].

analyse local phenomena is to use extremely refined theories, which lead to greater computational costs.

The variables kinematic models considered in this paper have been derived using different strategies. In the first benchmark, the refined theories are adopted in the area around the clamped section. For the thin-walled beam, the loaded area is the most suitable choice for a refinement of the kinematic model. Comparisons are made among results obtained with models adopting:

1. uniform Legendre expansions;
2. uniform Taylor expansions;
3. variable nodal HLE/HLE kinematics, indicated as HLE$m^{\times a}$-HLE$n^{\times b}$. In this case, two different HLE expansions are adopted. Both models can precisely discretize the geometry;
4. variable nodal HLE/TE kinematics, indicated as HLE$m^{\times a}$-TE$n^{\times b}$. These types of models are interesting when higher-order effects are restricted to a very limited part of the structure;
5. variable nodal HLE/HLE/TE kinematics, indicated as HLE$m^{\times a}$-HLE$n^{\times b}$-TE$s^{\times c}$. With these models, it is possible to tailor the extent of the local parts accurately.

In particular, the upper scripts denote the number of nodes of the beam elements adopting the corresponding kinematics. In each numerical case, the FE discretisation is fixed, and B4 elements are used along the y-axis to discretize the beam.
As an example, model HLE3$^{\times 10}$-HLE5$^{\times 4}$-TE2$^{\times 11}$ uses a third-order HLE model in the first ten nodes, a refined fifth-order HLE model in the central four nodes, and a second-order TE in the last eleven nodes.

4.1 End-Effects on Compact Sections

A cantilevered beam with a compact rectangular section is considered. The analysis was first proposed by Ghazouani and El Fatmi [51], and further investigated by Carrera *et al.* [52].

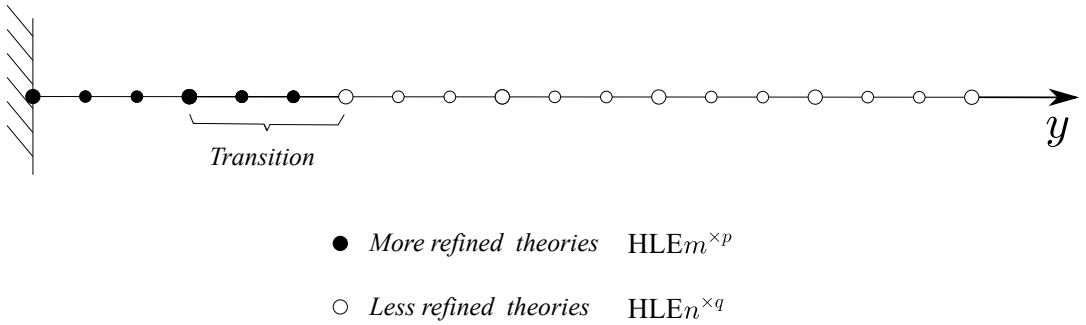

Figure 8: Cantilever beam with compact section: Simplified scheme of the NDK method.

The geometry is shown in Fig. 7. The height, h, is equal to 1 m; the ratio b/h is assumed to be equal to 0.5; and the aspect ratio L/h is assumed to be six, where L is the length of the beam. An orthotropic material is considered and its properties are: E_{11} = 206.80 GPa, $E_{22} = E_{33}$ = 5.17 GPa, $G_{12} = G_{13}$ = 3.10 GPa, G_{23} = 2.55 GPa, $\nu_{12} = \nu_{23} = \nu_{23}$ = 0.25. The beam is clamped at $y = 0$. Two loading conditions are considered: a concentrated load in the z-direction, F_z, and a concentrated load in the y-direction, F_y. See Figs. 7a and 7b, respectively. Both loads are posed in point A=$[0, L, 0]$ and are equal to 1 N. The analysis is focused on the end-effects caused by the boundary conditions. A comparison with higher-order beam theory [51], 3D FEM solution [51], and CUF-based solution [52] is given. In particular, a uniform fifth-order Taylor expansion is used as reference.
Forty B4 elements are adopted in the FEM discretization, as in the reference solution [52]. Several structural theories are used. First, uniform HLE1, HLE2, HLE3, and HLE5 models are adopted for comparison purposes. Then, NDK models are considered. In particular, Fig. 8 shows a simplified scheme of the NDK method. A local refinement is present near the clamped section, where HLE5 is adopted, while HLE1, HLE2, and HLE3 are used for the outer part of the beam.
Concerning the bending case, see Fig. 7a, axial stresses are evaluated along $[0, y, h/2]$. In this analysis, three different configurations of NDK models are used: HLE$5^{\times 21}$-HLE$n^{\times 100}$, HLE$5^{\times 41}$-HLE$n^{\times 80}$, and HLE$5^{\times 81}$-HLE$n^{\times 40}$. Table 1 compares the results of the models considered in this work with those from the literature. The stresses are calculated at $[0, 0, h/2]$. The relative error is given as follows:

$$err = \left|\left| \frac{\sigma_{yy}\,(\text{TE5[52]}) - \sigma_{yy}}{\sigma_{yy}\,(\text{TE5[52]})} \right|\right| \times 100 \tag{30}$$

The Degrees of Freedom (DOF) are reported in the last column. Figures 9 and 10 show the value of the axial tension σ_{yy} in the area close to the clamped section. Figure 9 compares the reference solutions and HLE5. Figures 10a, 10b, and 10c compare the results from the present NDK models with the results from the uniform kinematic models. Figure 11 shows the axial tension σ_{yy} in the cross-section (x, z) plane at $y = 0$ for HLE5, HLE5^{41}-HLE1^{80}, and HLE1. Figures 12a and 12b illustrate the trends for the strains ϵ_{xx} and ϵ_{yy}, respectively. For the sake of conciseness, only HLE5 and HLE1 kinematics are adopted. Some remarks can be outlined from these results:

1. The results show that the use of refined models, i.e. HLE5, is highly recommended to accurately study the boundary effect on σ_{yy}. Furthermore, the results confirm that end effects are limited to a length equal to three times the height of the cross section, as indicated by the literature results;

2. Models adopting HLE1 and HLE2 show similar results. Near the clamped section, the NDK models can approach the stresses calculated for the uniform kinematic HLE5 model. However, towards the transition zone, there is a leap and then the trend return to the reference solution;

3. Very accurate results are obtained if HLE5 and HLE3 are used together;

4. As expected, the larger is the area where the local model is used, more accurate the solution;

5. Figures 12a and 12b explain that the leaps presented in the axial stresses are due to the interfaces of two different kinematics expansions.

Concerning the traction case, see Fig. 7b, equivalent stresses are given in terms of $\sigma_t/\sigma_{yy}^{SV}$, where σ_t is equal to $(\sigma_{xx} + \sigma_{zz})/2$ and σ_{yy}^{SV} is equal to the force F_y divided by the area of the cross section. The stresses are evaluated along the line $[0, y, 0]$. In this analysis, two different configurations of NDK method are used: HLE5$^{\times 6}$-HLE$n^{\times 115}$ and HLE5$^{\times 21}$-HLE$n^{\times 100}$. Table 2 compares the results from the present models with a fifth-order Taylor theory [52]. The equivalent stresses are calculated at $[0, 0, 0]$. The relative error is shown in the third column. The formula is the same given in Eq. (30). The Degrees of Freedom (DOF) are indicated in the last column. Figures 13 and 14a show the value of the non-dimensional tension $\sigma_t/\sigma_{yy}^{SV}$ in the area close to the clamped section. In particular, Fig. 13 compares the reference solutions and the HLE5 model. Figures 14a, 14b, and 14c compare NDK models with uniform kinematic models. The following considerations can be drawn:

1. The uniform HLE5 model and the reference solution show a good agreement;

2. Since end-effects are confined to a restricted area, the local model can be applied in a portion of the beam equal to the thickness;

3. It is shown how HLE5$^{\times 21}$-HLE1$^{\times 100}$ and HLE5$^{\times 21}$-HLE2$^{\times 100}$ model can approximate the TE5 and HLE5 solutions accurately. On the other hand, HLE5$^{\times 6}$-HLE1$^{\times 115}$ and HLE5$^{\times 21}$-HLE2$^{\times 115}$ initially coincides with HLE5 and, after the transition, with HLE1 and HLE2, respectively.

4. It is sufficient to use only six local nodes when HLE5 and HLE3 are combined.

4.2 A thin-walled isotropic beam with C-shaped cross-section

The second benchmark is an isotropic thin-walled beam-like structure with a C-shaped cross-section. The geometrical properties are shown in Fig. 15. The length, L, is equal to 1 m, the width, a, and the height, h, are 0.1 m, and the thickness, t, is 0.005 m. This analysis was first proposed in Carrera *et al.* [53]. The structure is clamped at two ends and loaded by a concentrated load $F_z = 1000$ N at point A $= [a - t, \frac{L}{2}, \frac{h}{2}]$. The used material is aluminium alloy, and its properties are: $E = 71.7$ GPa and $\nu = 0.3$. Present models are compared with an ABAQUS 3D solution [53]. This model uses uniformly meshed second-order brick elements (C3D20R). In the 3D model, five layers of elements are used through the thickness of each wall, and two hundred elements are employed along the longitudinal direction.
Concerning the FEM discretization for the present CUF models, twenty-two B4 elements are adopted. The scheme is depicted in Fig. 16a. The mesh is more refined in the area nearby the

Model	$-\sigma_{yy}[Pa]$	err%	DOF
Literature			
TE5[52]	103.33	—	7623
Present-CUF			
HLE1	72.002	30.32	1452
HLE2	71.530	30.78	2904
HLE3	93.144	9.858	4356
HLE5	103.33	0.000	8349
HLE5$^{\times 41}$-HLE1$^{\times 80}$	101.38	1.887	3789
HLE5$^{\times 81}$-HLE1$^{\times 40}$	103.06	0.261	6069
HLE5$^{\times 41}$-HLE2$^{\times 80}$	101.39	1.887	4749
HLE5$^{\times 81}$-HLE2$^{\times 40}$	103.06	0.261	6549
HLE5$^{\times 21}$-HLE3$^{\times 100}$	103.40	0.068	5049
HLE5$^{\times 41}$-HLE3$^{\times 80}$	103.40	0.068	5709

Table 1: End effects caused by the boundary conditions on a cantilevered beam with compact rectangular section: bending loading and stresses evaluated in $[0, 0, h/2]$.

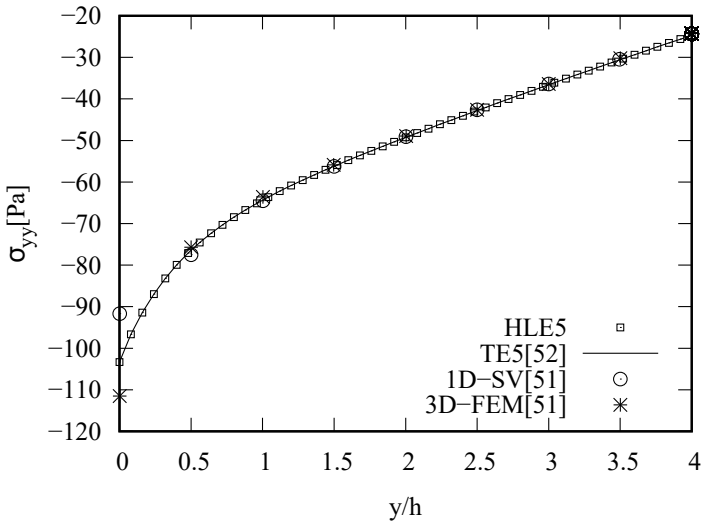

Figure 9: End effects caused by the boundary conditions on a cantilevered beam with compact rectangular section for reference solutions: bending loading and stresses evaluated in $[0, y, h/2]$.

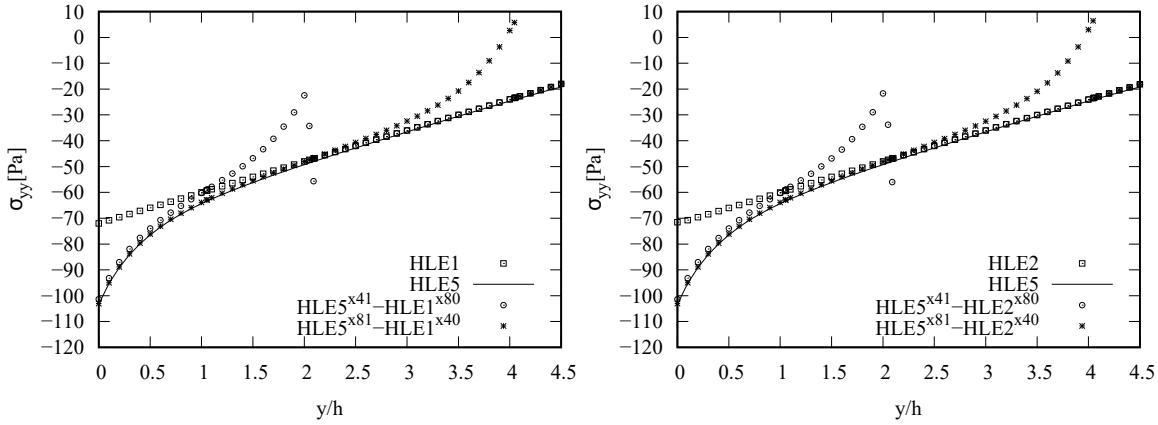

(a) HLE1 and HLE5 (b) HLE2 and HLE5

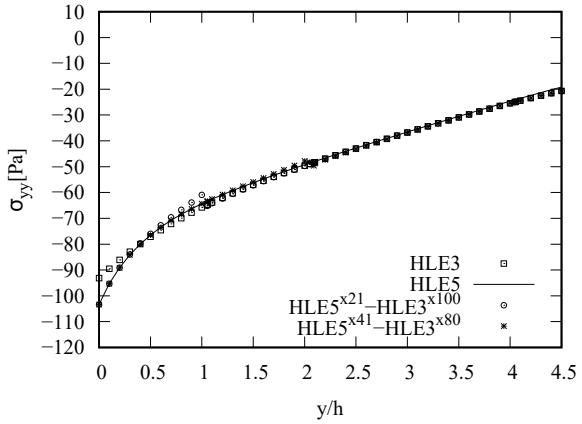

(c) HLE3 and HLE5

Figure 10: End effects caused by the boundary conditions on a cantilevered beam with compact rectangular section for NDK models: bending loading and stresses evaluated in $[0, y, h/2]$.

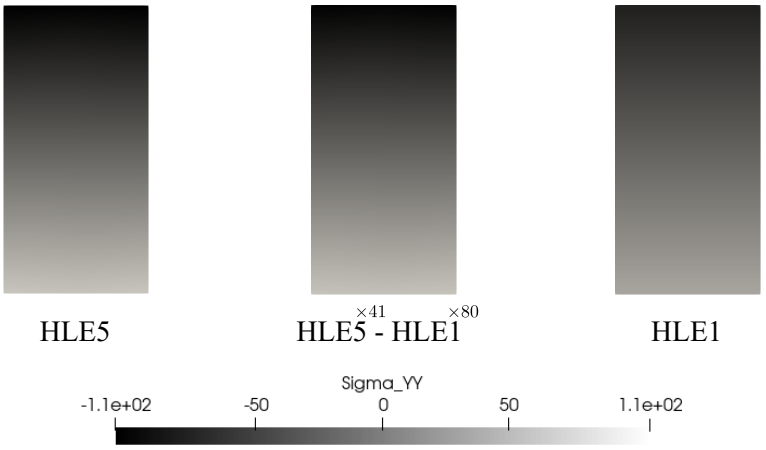

Figure 11: End effects caused by the boundary conditions on a cantilevered beam with compact rectangular section for reference solutions: bending loading and stresses evaluated in the plane $[x, 0, z]$.

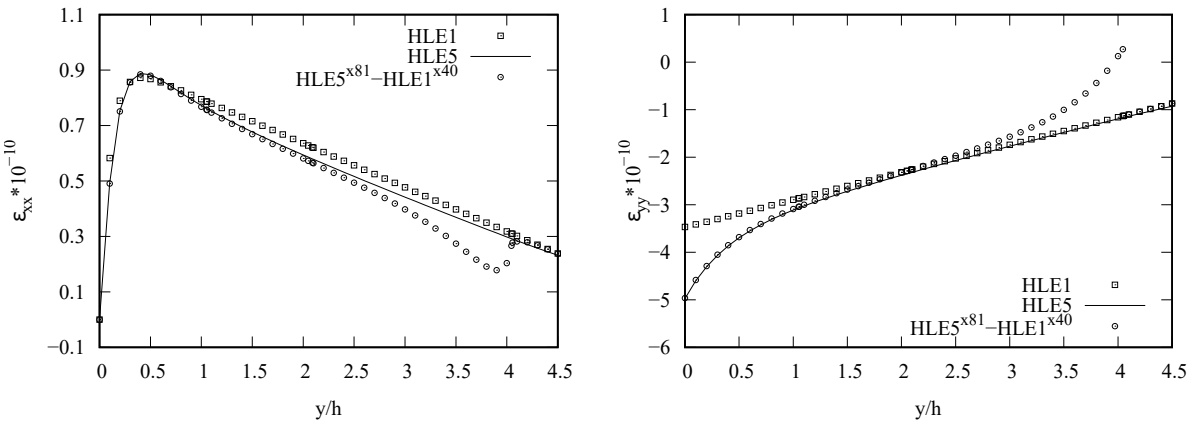

(a) HLE1 and HLE5 (b) HLE1 and HLE5

Figure 12: End effects caused by the boundary conditions on a cantilevered beam with compact rectangular section: bending loading and strains evaluated in $[0, y, h/2]$.

Model	$\sigma_t/\sigma_{yy}^{SV} \times 10^{-3}$	err%	DOF
Literature			
TE5[52]	8.350	—	7623
Present-CUF			
HLE1	8.334	0.192	1452
HLE2	8.212	1.653	2904
HLE3	8.215	1.617	4356
HLE5	8.350	0.000	8349
HLE5$^{\times 6}$-HLE1$^{\times 115}$	8.367	0.204	1794
HLE5$^{\times 21}$-HLE1$^{\times 100}$	8.355	0.060	2649
HLE5$^{\times 6}$-HLE2$^{\times 115}$	8.325	0.299	3174
HLE5$^{\times 21}$-HLE2$^{\times 100}$	8.349	0.012	3846
HLE5$^{\times 6}$-HLE3$^{\times 115}$	8.326	0.287	4554

Table 2: End effects caused by the boundary conditions on a cantilevered beam with compact rectangular section: traction loading and stresses evaluated in $[0, 0, 0]$; $\sigma_t = (\sigma_{xx} + \sigma_{zz})/2$.

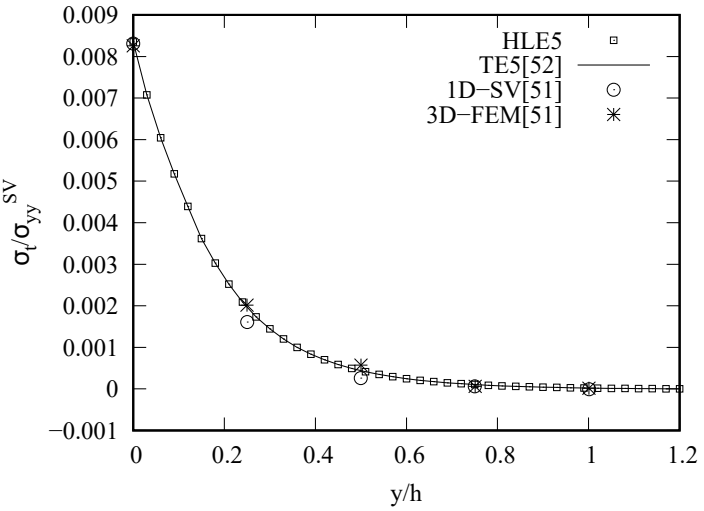

Figure 13: End effects caused by the boundary conditions on a cantilevered beam with compact rectangular section for reference solutions: traction loading and stresses evaluated in $[0, y, 0]$; $\sigma_t = (\sigma_{xx} + \sigma_{zz})/2$.

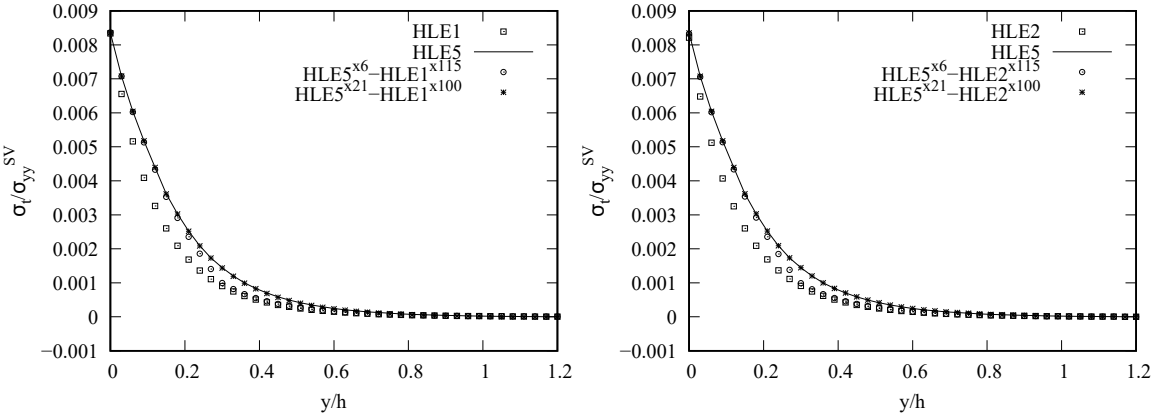

(a) HLE1 and HLE5

(b) HLE2 and HLE5

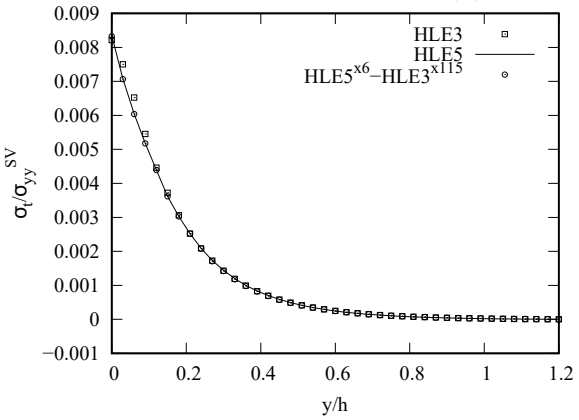

(c) HLE3 and HLE5

Figure 14: End effects caused by the boundary conditions on a cantilevered beam with compact rectangular section for NDK models: traction loading and stresses evaluated in $[0, y, 0]$; $\sigma_t = (\sigma_{xx} + \sigma_{zz})/2$.

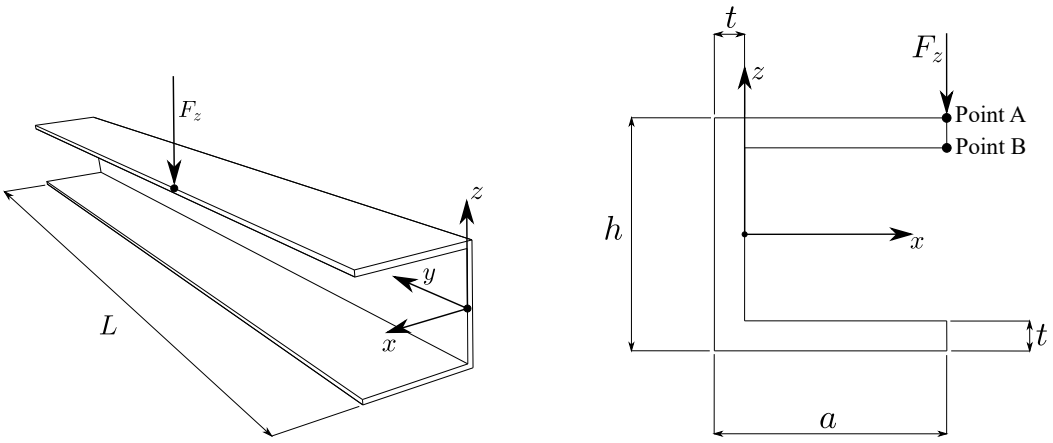

(a) Load (b) Mid-span section

Figure 15: Geometrical properties of the thin-walled isotropic beam with C-shaped cross-section. The study case is taken from [53].

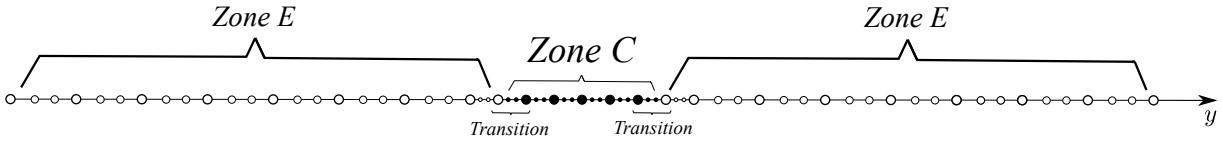

● *More refined theories* HLE$m^{\times 17}$

○ *Less refined theories* HLE$n^{\times 50}$ *or* TE$n^{\times 50}$

(a) Disposition of the structural theories.

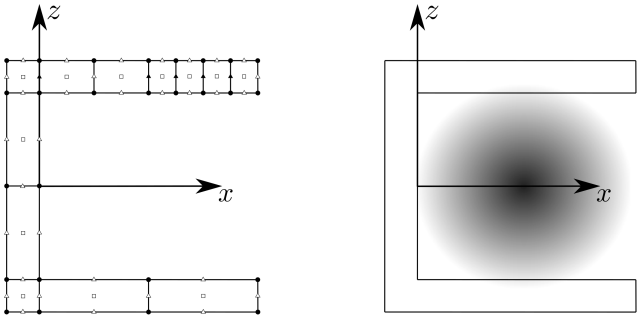

HLEm TEn

(b) Legendre and Taylor theories.

Figure 16: Thin-walled isotropic beam with C-shaped cross-section: Simplified scheme of the NDK method and adopted theories.

load. Furthermore, several structural theories are used. First, uniform HLE1, HLE2, HLE3, HLE4, and HLE5 models are adopted for comparison purposes. Then, a number of NDK models are proposed. For all the analyses, the scheme presented in Fig. 16a is used: Zone C has seventeen FE nodes, while Zone E comprises fifty nodes. Legendre- and Taylor-like expansions are used in the cross-section, see Fig. 16b.
Transverse displacement w and axial stresses σ_{yy} are evaluated along the line $[a-t, y, \frac{h}{2}-t]$. As a first assessment, different combinations of HLEm-HLEn schemes are considered to understand where the kinematic model refinement is needed. Table 3a shows the transverse displacements in point B. Table 3b shows the relative error towards the uniform model HLE5. Table 3c illustrates the relative error towards the 3D reference solution [53]. The following gives the relative error

$$\text{err}_{\text{Ref}} = \left|\left| \frac{\text{w (Ref)} - \text{w}}{\text{w (Ref)}} \right|\right| \times 100 \tag{31}$$

Tables 4a and 4b illustrate the DOFs adopted and the DOF reduction compared to the reference solution [53], respectively. The following gives the DOF reduction

$$\text{DOF Reduction} = \left|\left| \frac{\text{DOF (Ref)} - \text{DOF}}{\text{DOF (Ref)}} \right|\right| \times 100 \tag{32}$$

Furthermore, several HLEm-TEn schemes are analysed. In this case, the Legendre-like theories are used in the central zone, while Taylor-like kinematics are used in the external parts. Tables 5a shows the transverse displacements and Table 5b shows the relative error towards the uniform model HLE5. Table 5c illustrates the relative error towards the 3D reference solution [53]. Tables 6a and 6b the DOFs adopted and the DOF reduction compared to the reference solution [53], respectively.
In particular, HLE5 kinematics is used as a *local* theory in Zone C, while less refined theories, HLE1, and HLE2, are adopted as a *global theory*. Fig. 17 illustrates three contour plots for transverse displacements for HLE5, HLE5-HLE2, and HLE5-HLE1. Fig. 18a and Fig. 18b show the trends of displacements for uniform and NDK theories, respectively. Fig. 19a and Fig. 19b illustrate the axial stresses for uniform and NDK models, respectively.
Finally, three different kinematics are use used at the same time, see Fig. 20. In Zone C, seventeen nodes adopt a very refined theory, namely HLE5. Twenty-four FE nodes use HLE1 kinematics in ZONE E1. On the other hand, Zone E2, i.e twenty-six nodes adopt lower-order Taylor theories, namely TE2, TE3, or TE4. Table 7 compares the results of the reference result [53], uniform kinematics, and the NDK models in point B. Fig. 21a shows the transverse displacement along$[a-t, \frac{L}{2}, \frac{h}{2}-t]$, while Fig. 21b illustrates the axial stresses.
The analyses have demonstrated how the central part of the beam needs more advanced theories. A convergence analysis has been conducted to investigate the number of nodes in which a refined model HLE5 is required. Table 8 shows the results for the HLE5-HLE1 and HLE5-HLE2 models. Transverse displacements are analysed in Point B. The mesh discretization is fixed, as depicted in Fig. 16 a, while the local region with the refined model is progressively increased.
The following considerations can be drawn:

1. The effects of the point load are restricted to a small area. This allows to use refined theories in the area surrounding of the load, i.e. Zone C, while lower-order kinematics can be used near the clamped sections, i.e. Zone E;

2. Models HLE5 and HLE4 better fit the reference solution. Furthermore, it is shown that HLE5-HLEn and HLE4-HLEn yield good results with a strong DOF reduction.

3. The HLEm-TEn models have better computational efficiency than the uniform kinematic TE models. However, only Taylor polynomials with high order with HLE2 in Zone C can approach the HLE5 solution;

4. Figures 18 and 19 show how axial stresses are easier to calculate than transverse displacements. In fact, the stresses affect a limited area, while the effect area of displacements is wider;

5. Also, for the three-theories models, results have improved. Some discrepancies remain for the displacements. Regarding the axial stresses, the trend of NDK models near the point load is accurate. However, leaps in transition zones are present.

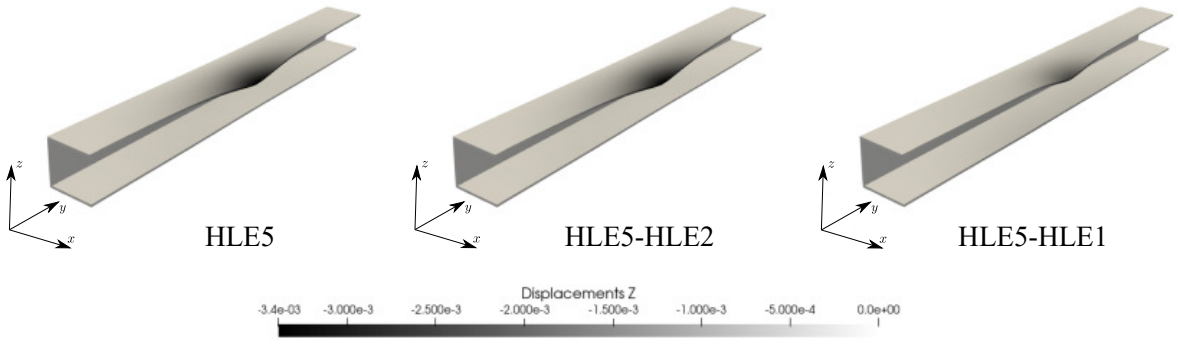

Figure 17: Thin-walled isotropic beam with C-shaped cross-section: contour plot of displacement of the beam with C-shaped section.

Zone E \ Zone C	HLE1	HLE2	HLE3	HLE4	HLE5
HLE1	1.279	2.309	2.346	2.359	2.364
HLE2	1.319	3.306	3.356	3.369	3.377
HLE3	1.321	3.323	3.378	3.391	3.400
HLE4	1.323	3.328	3.384	3.397	3.406
HLE5	1.323	3.332	3.388	3.401	3.409

(a) -w[mm]

w_{HLE5}=-3.409mm

Zone E \ Zone C	HLE1	HLE2	HLE3	HLE4	HLE5
HLE1	62.48	32.27	31.18	30.80	30.65
HLE2	61.31	3.024	1.555	1.173	0.9387
HLE3	61.25	2.523	0.9091	0.5280	0.2640
HLE4	61.19	2.376	0.7334	0.3520	0.0880
HLE5	61.19	2.259	0.6160	0.2347	0.00

(b) err[%] towards HLE5

$w_{ABAQUS[53]}$=-3.441mm

Zone E \ Zone C	HLE1	HLE2	HLE3	HLE4	HLE5
HLE1	62.83	32.90	31.82	31.44	31.30
HLE2	61.67	3.923	2.470	2.092	1.860
HLE3	61.61	3.429	1.831	1.453	1.192
HLE4	61.55	3.284	1.657	1.279	1.071
HLE5	61.55	3.168	1.540	1.163	0.9300

(c) err[%] towards ABAQUS[53]

Table 3: Thin-walled isotropic beam with C-shaped cross-section: displacements and errors for different combinations of HLEm-HLEn schemes.Displacements are calculated in Point B.

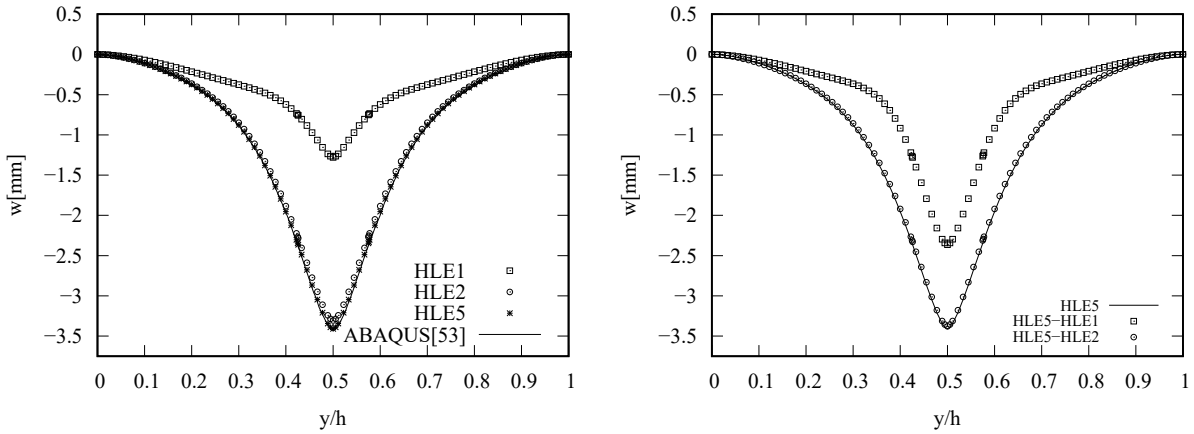

(a) Uniform models (b) NDK models

Figure 18: Thin-walled isotropic beam with C-shaped cross-section: variation of w along edge $(a-t, y, h/2-t)$ on the beam with C-shaped section for HLE models.

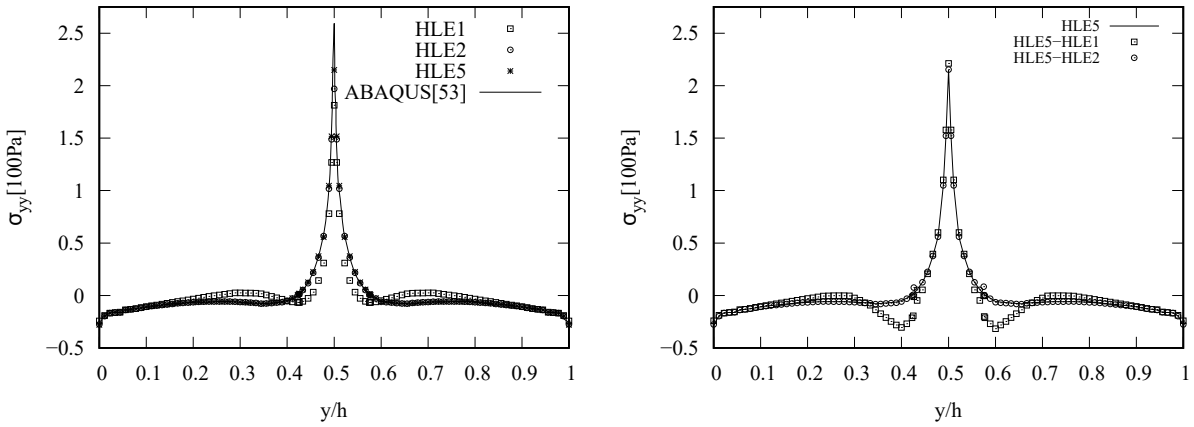

(a) Uniform models (b) NDK models

Figure 19: Thin-walled isotropic beam with C-shaped cross-section: variation of σ_{yy} along edge $(a-t, y, h/2-t)$ on the beam with C-shaped section for HLE models.

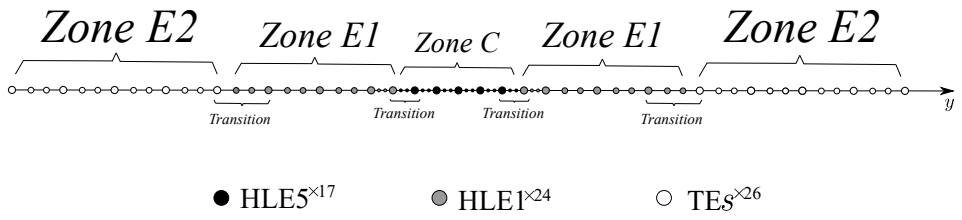

Figure 20: Thin-walled isotropic beam with C-shaped cross-section: Simplified Scheme of the NDK method for HLE5-HLE1-TEs models.

$DOF_{ABAQUS[53]}$=924399

Zone E \ Zone C	HLE1	HLE2	HLE3	HLE4	HLE5
HLE1	5226	7113	9000	11499	14610
HLE2	10776	12663	14550	17049	20160
HLE3	16323	18213	20100	22599	25710
HLE4	23676	25563	27450	29949	33060
HLE5	32826	34713	36600	39099	42210

(a) DOF

Zone E \ Zone C	HLE1	HLE2	HLE3	HLE4	HLE5
HLE1	99.44	99.23	99.03	98.76	98.42
HLE2	98.83	98.63	98.43	98.16	97.82
HLE3	98.23	98.03	97.83	97.56	97.22
HLE4	97.44	97.24	97.03	96.76	96.43
HLE5	96.45	96.25	96.03	95.77	95.43

(b) DOF Reduction [%]

Table 4: Thin-walled isotropic beam with C-shaped cross-section: DOF and DOF reduction respect to ABAQUS[53] for different combinations of HLEm-HLEn schemes.

Zone E \ Zone C	HLE1	HLE2	HLE3	HLE4	HLE5
TE2	0.5132	0.7651	0.7724	0.7727	0.7736
TE3	0.5847	0.8825	0.8922	0.8929	0.8941
TE4	0.9911	1.491	1.505	1.507	1.509
TE5	1.052	1.723	1.738	1.741	1.743
TE6	1.197	2.525	2.567	2.572	2.576
TE7	1.266	2.778	2.823	2.830	2.834
TE8	1.291	2.929	2.972	2.981	2.986

(a) -w[mm]

w_{HLE5}=-3.409mm

Zone E \ Zone C	HLE1	HLE2	HLE3	HLE4	HLE5
TE2	84.95	77.50	77.34	77.33	77.31
TE3	82.82	74.11	73.83	73.81	73.77
TE4	70.93	56.26	55.85	55.79	55.73
TE5	69.14	49.46	49.02	48.93	48.87
TE6	64.89	25.93	24.70	24.55	24.44
TE7	62.86	18.51	17.19	16.98	16.87
TE8	62.13	14.08	12.82	12.56	12.41

(b) err[%] towards HLE5

$w_{ABAQUS[53]}$=-3.441mm

Zone E \ Zone C	HLE1	HLE2	HLE3	HLE4	HLE5
TE2	85.09	77.71	77.55	77.54	77.52
TE3	83.01	74.35	74.07	74.05	74.02
TE4	71.20	56.57	56.26	56.20	56.15
TE5	69.43	49.93	49.49	49.40	49.35
TE6	65.21	26.62	25.40	25.25	25.14
TE7	63.21	19.27	17.76	17.76	17.64
TE8	62.48	14.88	13.63	13.37	13.22

(c) err[%] towards ABAQUS[53]

Table 5: Thin-walled isotropic beam with C-shaped cross-section: displacement and errors for different combinations of HLEm-TEn schemes. Displacements are calculated in Point B.

5 Conclusions

The present work proposed several refined beam FE theories with node-dependent kinematics thanks to the Carrera unified formulation. This approach is suitable for implementing global-local analysis. Hierarchical Legendre Expansions (HLE) are adopted as cross-section functions for the local refinement on the nodal level. In particular, it is now possible to use HLE with different polynomial orders in the same model. Also, Taylor expansions are used in global zone for certain analyses. Two well-known case studies were taken from open literature. Different kinds of boundary and load conditions were analysed. The results obtained with the developed NDK FEs were compared with analytical and numerical solutions. It can be highlighted that:

1. Combining HLE and NDK, the computational efficiency for the analysis of compact as well as thin-walled structures is improved;

$DOF_{ABAQUS[53]}$=924399

Zone E \ Zone C	HLE1	HLE2	HLE3	HLE4	HLE5
TE2	2226	4113	6000	8499	11610
TE3	2826	4713	6600	9099	12210
TE4	3576	5463	7350	9849	12960
TE5	4476	6363	8250	10749	13860
TE6	5526	7413	9300	11799	14910
TE7	6726	8613	10500	12999	16110
TE8	8076	9963	11850	14349	17460

(a) DOF

Zone E \ Zone C	HLE1	HLE2	HLE3	HLE4	HLE5
TE2	99.76	99.56	99.35	99.08	98.74
TE3	99.69	99.49	99.29	99.02	98.68
TE4	99.61	99.41	99.21	98.93	98.60
TE5	99.52	99.31	99.11	98.84	98.50
TE6	99.40	99.20	98.99	98.72	98.39
TE7	99.27	99.07	98.86	98.59	98.26
TE8	99.13	98.92	98.72	98.45	98.11

(b) DOF Reduction [%]

Table 6: Thin-walled isotropic beam with C-shaped cross-section: DOF and DOF reduction respect to ABAQUS[53] for different combinations of HLEm-TEn schemes.

Model	w[mm]	σ_{yy}[100 MPa]	DOF
Literature			
ABAQUS[53]	-3.441	2.598	924399
Present-CUF			
HLE5	-3.409	2.149	42210
HLE1	-1.279	1.813	5226
TE2[53]	-0.04912	-0.02217	1206
TE3[53]	-0.09333	0.07481	2010
TE4[53]	-0.5705	0.5681	3015
HLE5-HLE1-TE2	-1.972	2.144	13050
HLE5-HLE1-TE3	-2.032	2.155	13362
HLE5-HLE1-TE4	-2.195	2.195	13752

Table 7: Thin-walled isotropic beam with C-shaped cross-section: displacements and axial stresses for different combinations of HLE5-HLE1-TEs schemes. Both displacements and axial stresses are calculated in Point B.

2. Several structural theories can be adopted in the same model without additional coupling or superposition. In particular, different kinds of polynomials and polynomial orders can be joined;

3. The presented approach allows the local kinematic refinement to be carried out without changing the FE mesh;

4. HLE-HLE models can accurately obtain displacement and stress results.

References

[1] J. N. Reddy. On computational schemes for global-local stress analysis. *NASA, Langley Research Center, Computational Methods for Structural Mechanics and Dynamics, Part 1*, 1989.

[2] L. Euler. *Methodus inveniendi lineas curvas maximi minimive proprietate gaudentes sive solutio problematis isoperimetrici latissimo sensu accepti*, volume 1. Springer Science & Business Media, Berlin, Germany, 1952.

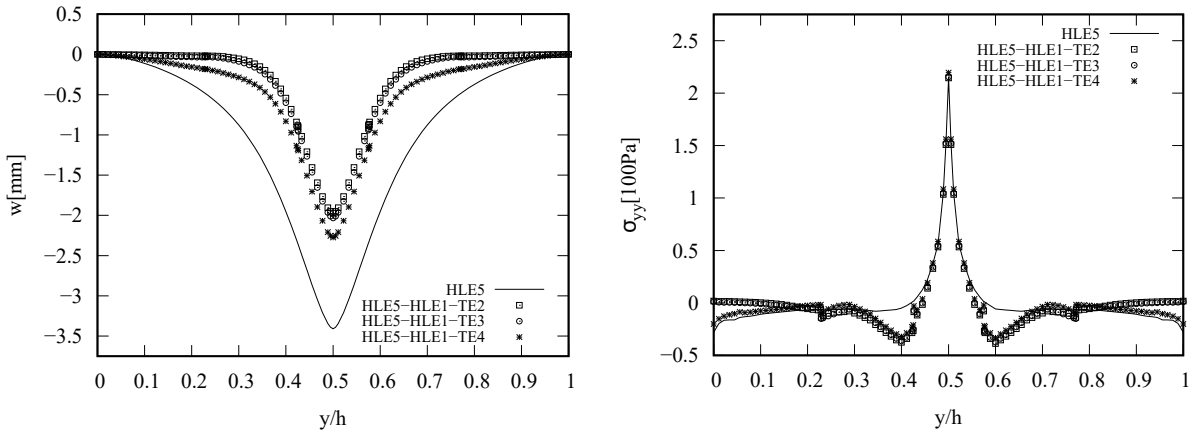

(a) Displacements (b) Axial stresses

Figure 21: Thin-walled isotropic beam with C-shaped cross-section: variation of w and σ_{yy} along edge $(a-t, y, h/2-t)$ on the beam with C-shaped section for HLE models.

$w_{ABAQUS[53]}$=-3.441mm $DOF_{ABAQUS[53]}$=924399; w_{HLE5}=-3.409mm DOF_{HLE5}=42210

	number of HLE5 nodes									
	3		7		11		17		21	
	w[mm]	DOF	w[mm]	DOF	w[mm]	DOF	w[mm]	DOF	w[mm]	DOF
HLE1	-1.420	6882	-1.681	9090	-1.970	11298	-2.364	14610	-2.552	16818
HLE2	-3.315	13986	-3.336	15750	-3.357	17514	-3.377	20160	-3.386	21924

Table 8: Thin-walled isotropic beam with C-shaped cross-section: convergence of displacements for different combinations of HLE5-HLE1 and HLE5-HLE2 schemes in Point B.

[3] S.P. Timoshenko. On the transverse vibrations of bars of uniform cross section. *Philosophical Magazine*, 43:125–131, 1922.

[4] V.V. Novozhilov. *Theory of elasticity*. Pergamon, Elmsford, 1961.

[5] R.K. Kapania and S. Raciti. Recent advances in analysis of laminated beams and plates. Part I: Shear effects and buckling. *AIAA journal*, 27(7):923–935, 1989.

[6] R.K. Kapania and S. Raciti. Recent advances in analysis of laminated beams and plates. Part II: Vibrations and wave propagation. *AIAA journal*, 27(7):935–946, 1989.

[7] E. Carrera, A. Pagani, M. Petrolo, and E. Zappino. Recent developments on refined theories for beams with applications. *Mechanical Engineering Reviews*, 2(2):14–00298–14–00298, 2015.

[8] V.Z. Vlasov. *Thin-walled elastic beams*. National Technical Information Service, 1984.

[9] P.O. Friberg. Beam element matrices derived from Vlasov's theory of open thin-walled elastic beams. *International Journal for Numerical Methods in Engineering*, 21(7):1205–1228, 1985.

[10] R.D. Ambrosini, J. D. Riera, and R. F. Danesi. A modified Vlasov theory for dynamic analysis of thin-walled and variable open section beams. *Engineering Structures*, 22(8):890–900, 2000.

[11] I. Mechab, N. El Meiche, and F. Bernard. Analytical study for the development of a new warping function for high order beam theory. *Composites Part B: Engineering*, 119:18–31, 2017.

[12] R. Schardt. Eine Erweiterung der Technischen Biegetheorie zur Berechnung prismatischer Faltwerke. *Der Stahlbau*, 35:161–171, 1966.

[13] V. L. Berdichevsky. Equations of the theory of anisotropic inhomogeneous rods. In *Doklady Akademii Nauk*, volume 228, pages 558–561. Russian Academy of Sciences, 1976.

[14] V. Giavotto, M. Borri, P. Mantegazza, G. Ghiringhelli, V. Carmaschi, G.C. Maffioli, and F. Mussi. Anisotropic beam theory and applications. *Computers & Structures*, 16(1):403–413, 1983.

[15] M. Živković, M. Kojić, R. Slavković, and N. Grujović. A general beam finite element with deformable cross-section. *Computer Methods in Applied Mechanics and Engineering*, 190(20):2651–2680, 2001.

[16] K. Yoon and P.-S. Lee. Modeling the warping displacements for discontinuously varying arbitrary cross-section beams. *Computers & Structures*, 131:56–69, 2014.

[17] H. Reda, S.E. Alavi, M. Nasimsobhan, and J.F. Ganghoffer. Homogenization towards chiral Cosserat continua and applications to enhanced Timoshenko beam theories. *Mechanics of Materials*, 155, 2021.

[18] S.E. Alavi, M. Sadighi, M.D Pazhooh, and J.F. Ganghoffer. Development of size-dependent consistent couple stress theory of Timoshenko beams. *Applied Mathematical Modelling*, 79:685–712, 2020.

[19] A. Bousselmi, Chaouachi F., J.F. Ganghoffer, and A. Zghal. Construction of new enriched beam models accounting for cross-section deformation and pinching. *International Journal of Mechanical Sciences*, 155:488–508, 2019.

[20] E. Carrera. C0 Reissner–Mindlin multilayered plate elements including zig-zag and interlaminar stress continuity. *International Journal for Numerical Methods in Engineering*, 39(11):1797–1820, 1996.

[21] E. Carrera and G. Giunta. Refined beam theories based on a unified formulation. *International Journal of Applied Mechanics*, 02(01):117–143, 2010.

[22] A. Airoldi, A. Baldi, P. Bettini, and G. Sala. Efficient modelling of forces and local strain evolution during delamination of composite laminates. *Composites Part B: Engineering*, 72:137–149, 2015.

[23] S.G. Haryadi, R.K. Kapania, and R.T. Haftka. Global/local analysis of composite plates with cracks. *Composites Part B: Engineering*, 29(3):271–276, 1998.

[24] T. Kubiak, Z. Kolakowski, J.Swiniarski, M. Urbaniak, and A. Gliszczynski. Local buckling and post-buckling of composite channel-section beams – numerical and experimental investigations. *Composites Part B: Engineering*, 91:176–188, 2016.

[25] A. K. Noor. Global-local methodologies and their application to nonlinear analysis. *Finite Elements in Analysis and Design*, 2(4):333–346, 1986.

[26] J. Fish, L. Pan, V. Belsky, and S. Gomaa. Unstructured multigrid method for shells. *International Journal for Numerical Methods in Engineering*, 39(7):1181–1197, 1996.

[27] W. Prager. Variational principles for elastic plates with relaxed continuity requirements. *International Journal of Solids and Structures*, 4(9):837–844, 1968.

[28] K. C. Park and C. A. Felippa. A variational principle for the formulation of partitioned structural systems. *International Journal for Numerical Methods in Engineering*, 47(1-3):395–418, 2000.

[29] E. Carrera, A. Pagani, and M. Petrolo. Use of Lagrange multipliers to combine 1D variable kinematic finite elements. *Computers & Structures*, 129:194–206, 2013.

[30] M. A. Aminpour, J. B. Ransom, and S. L. McCleary. A coupled analysis method for structures with independently modelled finite element subdomains. *International Journal for Numerical Methods in Engineering*, 38(21):3695–3718, 1995.

[31] J. B. Ransom. *On multifunctional collaborative methods in engineering science*. National Aeronautics and Space Administration, Langley Research Center, 2001.

[32] F. Brezzi and L. D. Marini. The three-field formulation for elasticity problems. *GAMM-Mitteilungen*, 28(2):124–153, 2005.

[33] P.J. Blanco, R.A. Feijóo, and S.A. Urquiza. A variational approach for coupling kinematically incompatible structural models. *Computer Methods in Applied Mechanics and Engineering*, 197(17):1577–1602, 2008.

[34] P. Blanco, P. Gervasio, and A. Quarteroni. Extended variational formulation for heterogeneous partial differential equations. *Computational Methods in Applied Mathematics*, 11(2):141–172, 2011.

[35] B. H. Dhia. Problèmes mécaniques multi-échelles: la méthode Arlequin. *Comptes Rendus de l'Académie des Sciences - Series IIB - Mechanics-Physics-Astronomy*, 326(12):899–904, 1998.

[36] H. B. Dhia and G. Rateau. The arlequin method as a flexible engineering design tool. *International Journal for Numerical Methods in Engineering*, 62(11):1442–1462, 2005.

[37] F. Biscani, G. Giunta, S. Belouettar, E. Carrera, and H. Hu. Variable kinematic beam elements coupled via Arlequin method. *Composite Structures*, 93(2):697–708, 2011.

[38] F. Biscani, G. Giunta, S. Belouettar, E. Carrera, and H. Hu. Variable kinematic plate elements coupled via arlequin method. *International Journal for Numerical Methods in Engineering*, 91(12):1264–1290, 2012.

[39] H. Hu, S. Belouettar, M. Potier-Ferry, and E. M. Daya. Multi-scale modelling of sandwich structures using the Arlequin method Part I: Linear modelling. *Finite Elements in Analysis and Design*, 45(1):37–51, 2008.

[40] H. Hu, S. Belouettar, M. Potier-Ferry, E. M. Daya, and A. Makradi. Multi-scale nonlinear modelling of sandwich structures using the Arlequin method. *Composite Structures*, 92(2):515–522, 2010.

[41] S. Klarmann, J. Wackerfuß, and S. Klinkel. Coupling 2D continuum and beam elements: a mixed formulation for avoiding spurious stressess. *Computational Mechanics*, 70(6):1145–1166, 2022.

[42] A.R. Hartloper, A. de Castro e Sousa, and D.G. Lignos. Warping-inclusive kinematic coupling in mixed-dimension macro models for steel wide flange beam columns. *Journal of Structural Engineering*, 148(2), 2022.

[43] E. Zappino and E. Carrera. Multidimensional model for the stress analysis of reinforced shell structures. *AIAA Journal*, 56(4):1647–1661, 2018.

[44] E. Carrera and E. Zappino. One-dimensional finite element formulation with node-dependent kinematics. *Computers & Structures*, 192:114–125, 2017.

[45] G. Li, A.G. de Miguel, A. Pagani, E. Zappino, and E. Carrera. Finite beam elements based on Legendre polynomial expansions and node-dependent kinematics for the global-local analysis of composite structures. *European Journal of Mechanics - A/Solids*, 74:112–123, 2019.

[46] F. Moleiro, E. Carrera, E. Zappino, G. Li, and M. Cinefra. Layerwise mixed elements with node-dependent kinematics for global–local stress analysis of multilayered plates using high-order legendre expansions. *Computer Methods in Applied Mechanics and Engineering*, 359:112764, 2020.

[47] B. Szabo and I. Babuška. *Finite element analysis*. John Wiley & Sons, 1991.

[48] M. Abramowitz and I.A. Stegun. *Handbook of mathematical functions with formulas,*. Dover Publications, 1964.

[49] K.J. Bathe. *Finite Element Procedure*. Prentice hall, Upper Saddle River, New Jersey, USA, 1996.

[50] E. Carrera, M. Cinefra, M. Petrolo, and E. Zappino. *Finite element analysis of structures through unified formulation*. John Wiley & Sons, 2014.

[51] N. Ghazouani and R. El Fatmi. Higher order composite beam theory built on Saint-Venant's solution. Part-II: Built-in effects influence on the behavior of end-loaded cantilever beams. *Composite Structures*, 93(2):567–581, 2011.

[52] E. Carrera, M.Petrolo, and E. Zappino. Performance of CUF approach to analyze the structural behavior of slender bodies. *Journal of Structural Engineering*, 138(2):285–297, 2012.

[53] E. Carrera, E. Zappino, and G. Li. Finite element models with node-dependent kinematics for the analysis of composite beam structures. *Composites Part B: Engineering*, 132:35–48, 2018.